

Random tiling quasicrystals in three dimensions

W. Ebinger, J. Roth, H.-R. Trebin,
 Institut für Theoretische und Angewandte Physik
 Universität Stuttgart
 Pfaffenwaldring 57
 70550 Stuttgart, Germany
 (October 18, 2019)

Three-dimensional icosahedral random tilings with rhombohedral cells are studied in the semi-entropic model. We introduce a global energy measure defined by the variance of the quasilattice points in the orthogonal space. The internal energy, the specific heat, the configuration entropy and the sheet magnetization (as defined by Dotera and Steinhardt [Phys. Rev. Lett. **72** (1994) 1670]) have been calculated. The specific heat shows a SCHOTTKY anomaly which might indicate a phase transition from an ordered quasicrystal to a random tiling. But the divergence with the sample size as well as the divergence of the susceptibility are too small to pinpoint the phase transition conclusively. The self-diffusion coefficients closely follow an ARRHENIUS law, but show plateaus at intermediate temperature ranges which are explained by energy barriers between different tiling configurations due to the harmonic energy measure. There exists a correlation between the temperature behavior of the self-diffusion coefficient and the frequency of vertices which are able to flip (simpletons). Furthermore we demonstrate that the radial distribution function and the radial structure factor only depend slightly on the random tiling configuration. Hence, radially symmetric pair potentials lead to an energetical equidistribution of all configurations of a canonical random tiling ensemble and do not enforce matching rules.

I. INTRODUCTION

The stability of quasicrystals has been a riddle since their discovery in 1982. Do they form stable or metastable states? Are they stable only at high temperatures? Is the stability due to energetic or due to entropic reasons? The random tiling model of quasicrystals is an abstraction which deals with rigid tiles, thereby neglecting thermal fluctuations and the phonon degrees of freedom. The only dynamic process is the local rearrangement of tiles, called “flips”, “umklapps”, “zipper” moves, depending on the type of tiles and symmetries. The random tiling model has been proposed by Elser [1] and has been studied intensively in recent years. The first author dealing with random rhombohedral tilings in three dimensions was Tang [2] who was interested in diffuse scattering and phason elastic constants. Strandburg [3] calculated the configurational entropy. The state of the art of random tilings was reviewed by Henley [4]. Ebinger [5] studied random tilings at infinite temperatures. Dotera and Steinhardt [6] introduced the concept of sheet magnetization as an order parameter to describe the randomness. Interest in random tilings was renewed by Kalugin and Katz [7] through the new process of flip diffusion. This property has been studied by Jarić and Sørensen [8,9] at infinite temperature, and by Joseph [10] and Gähler [11] at finite temperatures. Meanwhile for the energetic interaction of the tiles many different sets of matching rules exist.

In the present work we first deal with quantities that allow to characterize a random tiling. We are especially interested in the atomic plane and line structures important for example for ion channeling (Sec. III). Energy measures (Sec. IV) are discussed and a new method for generating non-equilibrium quasicrystals (Sec. V) is established. The possibility of a random tiling equilibrium phase transition is studied in Sec. VI. Structure functions are introduced in Sec. VIA, and results concerning a special “harmonic energy measure” as defined in Sec. IV are presented in Sec. VIII. Conclusions are drawn in Sec. IX.

II. DEFINITIONS

Quasicrystals can be described as cuts through higher-dimensional periodic crystals. The additional dimensions are addressed as orthogonal space \mathbb{E}^\perp . Quasilattice points \mathbf{x} in the physical space \mathbb{E}^\parallel can uniquely be lifted to the higher-dimensional space $\mathbf{X} = \Pi_\parallel^{-1}\mathbf{x}$ and then be projected onto the orthogonal space by $\mathbf{y} = \Pi_\perp(\mathbf{X})$ ($\Pi_\parallel + \Pi_\perp = id$ in a proper normalization). The infinitely extended quasilattice thus is contracted into a finite volume called “acceptance domain” or “atomic hypersurface”. The whole procedure of lifting and projecting into the orthogonal space is called “dualization” $\mathbf{y} = \Pi_\perp \circ \Pi_\parallel^{-1}\mathbf{x}$ of the quasilattice. The higher-dimensional embedding generates new degrees of freedom in addition to the ordinary phonons in periodic crystals, denoted “phasons”.

The icosahedral quasilattice lifted into higher-dimensional space forms a three-dimensional hypersurface, called “de-Bruijn-hypersurface” or “Weiringia roof” [12]. The hypersurface fluctuates around an average hyperplane $\mathbf{h}(\mathbf{x}) = \mathbf{h}_0 + \varepsilon_{global}\mathbf{x}$. The constant quantity

$$\varepsilon_{global} := \nabla_\parallel \otimes \mathbf{h}(\mathbf{x}) = const$$

is called “global phason strain” and describes the deviation of the slope of the average hyperplane $\mathbf{h}(\mathbf{x})$ from the slope of the physical space. In the case of exact icosahedral symmetry the average hyperplane is running parallel to the physical space and thus $\varepsilon_{global} = 0$.

Long-wavelength deviations from the hypersurface are denoted as “phason fluctuations” and are described in a continuum picture by a phason strain tensor

$$\varepsilon(\mathbf{x}) := \nabla_\parallel \otimes \mathbf{h}(\mathbf{x}) .$$

According to Henley [13] the fluctuations are governed by a free energy depending quadratically on the phason strain:

$$F = \int d^d\mathbf{x} \text{trace}(\varepsilon(\mathbf{x}) \otimes \varepsilon(\mathbf{x})^\mathbf{T}) .$$

The dimension d of physical space is equal to three for icosahedral quasicrystals.

The present work deals with the three-dimensional Ammann-Kramer-Penrose tiling and its randomizations. This tiling consists of two different elementary cells, the “oblate” and “prolate” rhombohedron. Both of them appear in ten different orientations in the tiling. The six rational linearly independent unit edge vectors \mathbf{t}_i may be defined as $\mathbf{t}_\alpha = \frac{\sqrt{2}}{5}(\cos \frac{2}{5}\pi\alpha, \sin \frac{2}{5}\pi\alpha, \frac{1}{2})$ ($\alpha=0,\dots,4$) and $\mathbf{t}_5=(0,0,1)$. The atomic hypersurface is a rhombic triacontahedron of icosahedral symmetry. The tiling exhibits, among others, a vertex representing lattice points where two prolate and two oblate rhombohedra meet. It is denoted “simpleton vertex”. The outer shape of the cells, which touch this vertex, is a rhombic dodecahedron. If the dodecahedron is kept fixed, two possibilities exist to fill it with tiles. The exchange of one configuration by the other is a “flip”. The lattice point jumps a distance which is 0.650 of the edge length of the rhombohedra (Fig. 1). Any non-ordered space filling arrangement of rhombohedra without gaps or overlaps is called a “random tiling”.

III. RANDOM TILING CHARACTERIZATION

A. Variance

Any random tiling may be characterized by the mean square deviation of the point distribution from the center of mass in the orthogonal space. The variance is defined by

$$\Omega = \frac{1}{N} \sum_{j=1}^N \left| \mathbf{y}_j - \frac{1}{N} \sum_{i=1}^N \mathbf{y}_i \right|^2 = \frac{1}{N} \sum_{j=1}^N |\mathbf{y}_j - \mathbf{y}_0|^2 \quad . \quad (1)$$

N is the number of quasilattice sites and \mathbf{y}_0 is the average of the position vectors \mathbf{y}_i of all dual quasilattice sites. The bigger the phason fluctuations are the larger is the disorder and therefore the random tiling parameter Ω . The averaged value in the pure entropic random tiling ensemble amounts to 1.73 ± 0.01 [2].

B. Vertex frequency

The lattice points of a quasicrystal can be characterized by their local environment. The number of rhombohedra adjacent to a lattice point in an icosahedral quasilattice varies from 4 to 20, the number of edges from 4 to 12. There are 24 “canonical” or “allowed” vertices, but 5450 vertices may occur in a random tiling. Vertices where two identical rhombohedra meet are called “crystallographic”. Without them the number of vertices is reduced to 360 [14].

In the two-dimensional Penrose tiling each flip generates non-canonical vertices. There the knowledge of the vertices suffices to distinguish between ideal and random tilings. This statement is not valid in three dimensions. There are some flips possible in the rhombohedra tiling which only change the frequency of vertices without introducing forbidden ones. If the degree of randomization has reached a certain level the number of forbidden vertices is going to rise rapidly.

C. Sheet magnetization

The frequency of the simpleton is 23.61% in the ideal rhombohedra tiling. The simpletons are arranged in two-dimensional layers perpendicular to the two-fold symmetry axis. Due to the two possibilities to pack the rhombohedra into the simpleton there are two positions for the internal lattice point. The positions may be called “up” and “down” and attributed a spin value $S = \pm 1$. In the ideal rhombohedra tiling all the spins in a certain layer carry spin +1 or -1. Dotera and Steinhardt [6] have defined a sheet magnetization of value 1 using a proper summation rule. In a random tiling the sheets also exist, but the magnetization is reduced since the spins in one layer are not all aligned. The collection of all sheets can therefore be regarded as a two-dimensional Ising model with a variable number of spins. There is, however, no interaction leading to an Ising Hamiltonian. The sheet magnetization simply is being used as an order parameter which may indicate an order-disorder transition. The number of spins is not constant as in a standard Ising system. The susceptibility is given by

$$\chi = \frac{1}{T} \langle N_D \rangle \left(\left\langle \frac{M^2}{N_D^2} \right\rangle - \left\langle \frac{M}{N_D} \right\rangle^2 \right) \quad .$$

N_D is the number of the dodecahedra and therefore the number of the “spins” in the patch. This equation replaces the more cumbersome definition used in [6].

D. Tube and slab structures

In the three-dimensional icosahedral rhombohedra tiling special tube structures, denoted “worms”, exist along two-fold axes (Fig. 2). They are formed of stacks of rhombohedra which have one type of face in common, perpendicular to the two-fold axis. In addition to the tube structures there are slab structures perpendicular to a five-fold direction. The slabs are formed by rhombohedra which have one type of edge in common (parallel to the five-fold axis). The projection of the slab structures onto the plane perpendicular to the appropriate five-fold direction

yields generalized Penrose tilings in two dimensions. These tube and slab structures exist in ideal tilings as well as in random tilings.

E. Plane and chain density diagrams

Atoms in crystals are arranged in lattice planes characterized by a normal vector of rational components (the Miller indices), and in lattice chains with a rational direction vector. This fact also holds for quasicrystals. The lattice planes or chains of a fixed direction in a crystal all are equivalent to one another in the simple cases (or they fall into a small number of classes). This is not true for a quasicrystal: For example, the density of atoms in a certain plane does not only depend on the orientation of the plane but also on its position. The basic theory can be found in Ref. [15]. The plane and chain structures have been studied in Ref. [16,17].

As described in Sec. II it is possible to lift the quasilattice points into the higher-dimensional space and to project them onto the orthogonal space. Points in the same physical plane are situated in the same plane in the orthogonal space [15], and points on one chain in the physical space will lie on one chain in the orthogonal space, in the ideal tiling within the acceptance domain, respectively.

To describe densities of atoms in the planes of our (primitively decorated) quasicrystal, we use the function $A_s(\xi^\perp)$. The index s shall indicate a two-, three- or five-fold symmetry direction. ξ^\perp is the coordinate of position of a plane in the direction parallel to its normal and is the dual of the height ξ^\parallel of the selected plane in the physical space (with respect to the origin for example). $A_s(\xi^\perp)$ is proportional to the area of the intersection plane at ξ^\perp through the triacontahedral acceptance domain in the ideal tiling, since the density of points is 1 in the domain and 0 outside.

For random tilings we have to use another definition. The area of $A_s(\xi^\perp)$ at the position ξ^\perp in \mathbb{E}^\perp is proportional to the plane decoration density $\rho_{F,s}(\xi^\parallel[\xi^\perp]) =: \rho_{F,s}(\xi^\parallel)$ of the corresponding plane $\xi^\parallel = \text{const}$ in physical space. The index F denotes plane densities.

In the case of an ideal quasicrystal, the values of $A_s(\xi^\perp)$ are between 0 and a maximal value for five-fold and three-fold directions (Fig. 3). In the five-fold case the function has a constant plateau since the corners of the intersection polygon are formed by edges of the triacontahedron perpendicular to the plane. In the two-fold case the minimal value of $A_s(\xi^\perp)$ is greater than zero, since the smallest intersection polygons coincide with the surface-rhombi of the triacontahedron parallel to the intersection plane. To obtain the average density of atoms in a plane one has to calculate the mean value of the area of the intersection polygons. It is equivalent to the volume of the triacontahedron divided by the diameter Δ_s of the triacontahedron along the direction s . Then the mean value of the plane density is:

$$\bar{\rho}_{F,s} \propto \bar{A}_s = \frac{V_{Tria}}{\Delta_s} .$$

For channeling experiments one is interested in the frequency $H(\rho_{F,s})$ of planes perpendicular to s with a plane density $\rho_{F,s}$ in the interval $\delta\rho_{F,s}$. Wherever the intersection function $A_s(\xi^\perp) \propto \rho_{F,s}(\xi^\parallel)$ is flat, there are many $\xi^\parallel[\xi^\perp]$ values for $\rho_{F,s}$ inside of $\delta\rho_{F,s}$. If the slope is large, the number of planes with this density is small. The densities $H(\rho_{F,s})$ are obtained from the values $\rho_{F,s}$ by a subdivision of the $\rho_{F,s}$ axis into intervals $\delta\rho_{F,s}$ of equal length and calculating for each interval $\delta\rho_{F,s}$ the length of the inverse image on the ξ^\perp -axis. Since the triacontahedron is a convex polyhedron and centrosymmetric, the function $A_s(\xi^\perp)$ is monotonously growing in one half of the interval Δ_s and monotonously decreasing in the other. Therefore one can calculate the first derivative of the inverse image (that means $\delta\rho_{F,s} \rightarrow 0$) in one half and set it proportional to $H(\rho_{F,s})$ which hence is $\xi^\perp'(A_s)$. Since $A_s(\xi^\perp)$ has horizontal lines and kinks, $H(\rho_{F,s})$ possesses poles and jumps.

Similarly as the plane structures one also finds chains in the quasicrystal. The direction again is denoted by s , the position in the perpendicular space now is characterized by a two-dimensional parameter $\{\eta^\perp, \zeta^\perp\} = \text{const}$ with its counterpart in the physical space at $\{\eta^\parallel, \zeta^\parallel\} = \text{const}$. The

chain density $\rho_{l,s}(\eta^\perp, \zeta^\perp)$ at $[\eta^\perp, \zeta^\perp]$ is proportional to the intersection distance $w_s(\eta^\perp, \zeta^\perp)$ of the dual line through the triacontahedron. The index l denotes line densities.

To obtain the average chain density for a given direction s one has to calculate the average intersection length \bar{w}_s . It is equivalent to the volume of the triacontahedron divided by the area $\Phi_{Tria,s}$ of the triacontahedron projected onto the $\eta^\perp \zeta^\perp$ -plane:

$$\bar{\rho}_{l,s} \propto \bar{w}_s = \frac{V_{Tria}}{\Phi_{Tria,s}} .$$

It is also possible to calculate frequencies of the chain densities. The $\rho_{l,s}$ -axis is divided up into intervals $\delta\rho_{l,s}$. For each $\rho_{l,s}$ the respective inverse image area in the $\eta^\perp \zeta^\perp$ -plane is calculated for the values $w_s(\eta^\perp, \zeta^\perp)$ belonging to $\rho_{l,s}$ and $\delta\rho_{l,s}$. The total area is proportional to $H(\rho_{l,s})$. The chain intersection function $w_s(\eta^\perp, \zeta^\perp)$ is piecewise linear due to the flatness of the surface rhombs of the triacontahedron. It decreases monotonously in radial direction from the center of the interface $\phi_{Tria,s}$ to the boundaries.

The frequency function may be derived analytically in the following way: The origins of the coordinate ξ^\perp parallel to the symmetry axis \hat{s} and of the coordinates η^\perp and ζ^\perp in the plane perpendicular to \hat{s} are chosen in such a way that it coincides with the projection of the center of the triacontahedron. Then we compute the area of the interface $F(\xi^\perp)$ of the triacontahedron with the same ξ^\perp as a function of ξ^\perp for the half space $\xi^\perp \geq 0$. Due to the convexity of the triacontahedron the function $F(\xi^\perp)$ decreases monotonously. From the inverse of the derivative of $F(\xi^\perp)$ ($\delta\rho_{l,s} \rightarrow 0$) one obtains a function which is piecewise linear, has discontinuities and can be identified with the density function $H(\rho_{l,s})$ (Fig. 4).

IV. ENERGY MEASURES

A. Models of stability

Several models currently exist to explain the stability of quasicrystals. In the deterministic energy model the internal energy U represents the thermodynamically stabilizing factor. Microscopic forces lead to matching rules [12] or overlapping cluster energies [18,19] that favour an ideal quasicrystalline tiling. In the non-deterministic entropic model stabilized by the entropy S no matching rules exist but the cells of the tiling do not leave any gaps and do not overlap. This is the random tiling model. In between is the semi-entropic model which is described by a free energy with contributions from internal energy and entropy:

$$F(T) = U(T) - TS(T) . \quad (2)$$

The purely energetic model can be regarded as a low-temperature limit, the purely entropic model as a high-temperature limit of the semi-entropic model.

B. Properties of energy measures

The ideal quasilattice without any violation of matching rules represents the ground state of the energy model, taken at $T=0$. At finite temperatures thermally activated flips exist, mediating the transition between neighbouring states. The transition probability is given by the Boltzmann factor, which depends on the energy measure chosen.

In this work we deal with the canonical random tiling ensembles. All configurations of an ensemble have the same volume and the same number of vertices due to a constant average slope of the de-Bruijn-hypersurface. The energy of the system is the ensemble average. The pure entropic random tiling model, on the other hand, is specialized for microcanonical ensembles, since all configurations have the same energy. Starting from the occupation distribution of the energy

levels of a canonical random tiling ensemble in the thermodynamic equilibrium we can calculate the internal energy $U(T)$ as the ensemble average $U = \langle E \rangle$ of the instantaneous energy E . The specific heat $C_V(T)$ can be derived from the variance of the occupied energy levels by the fluctuation-dissipation theorem

$$\langle (\delta E)^2 \rangle = \langle E^2 \rangle - \langle E \rangle^2 = k_B T^2 C_V = \frac{\partial U}{\partial T} .$$

The temperature-dependent internal energy and the specific heat are governed by the intrinsic properties of the system and the selected energy measure. The temperature dependence of the entropy density $s(T)$ (precisely: entropy per quasilattice site¹) is given by the thermodynamical integration of c_V :

$$s(T) = s_V(T) + \int_0^T dT' \frac{c_V(T')}{T'} + s_0 . \quad (3)$$

$s_V(T)$ is the entropy contribution of a change of volume. It vanishes for canonical random tilings. c_V is the isochoric specific heat and $s_0 := s(T=0)$ the ground state entropy. At $T \rightarrow \infty$ we are in the limit of the pure random tiling model and we get the configuration entropy $s(T=\infty) =: s_\infty$. The temperature variation of the specific heat depends on the energy measure, but not s_∞ . If one is interested only in the configuration entropy s_∞ , then the specific choice of the energy measure has no physical relevance if the first three of the following four conditions are fulfilled:

1. The energy of any configuration is unique.
2. The quasiperiodic reference tiling is a ground state.
3. The energy measure is limited from above.
4. The entropy of the ground state vanishes or is easy to calculate.

The first condition requires an exact law to determine the energy of any microstate. The energy of a fixed microstate must not depend on how it is generated. Two configurations that differ only by a rigid translation have to be energetically identical.

Especially global energy measures are endangered to violate the second condition and to render the quasiperiodic reference state unstable at $T = 0$. The third condition is a requirement for the integrability of $\frac{c_V(T)}{T}$ as a function of T . If the energy measure is not limited, uncontrolled fluctuations of the energy in the high-temperature limit may exist. If they vary stronger than quadratic with T then

$$\frac{\langle (\delta E)^2 \rangle}{T^2}$$

diverges and with it c_V as $T \rightarrow \infty$.

The last condition need not be met but is recommended for practical purposes. The ground state entropy s_0 represents the number of states energetically equivalent to the quasiperiodic ground state. Since it is often complicated to calculate the ground state entropy it is useful to choose an energy measure where s_0 vanishes or is easy to deduce. An example of a complicated

¹Large letters indicate total quantities, small letters denote a quantity per vertex. For periodic approximants with rhombohedral cells the number of cells and vertices is identical.

case of non-vanishing contribution s_0 has been presented by Baake and Joseph [20] for a two-dimensional octagonal quasicrystal. The locally defined energy measure is 0 for the canonical vertices but positive for forbidden vertices and depends on the vertex type. Unfortunately there exist configurations which are not quasiperiodic, although they do not exhibit forbidden vertices. As a consequence 44% of the total entropy are contributed by the ground state.

An example for a globally defined energy measure with an easily calculable ground state entropy is the ansatz of a harmonic oscillator potential in the orthogonal space as applied in this work. The energy is the sum of the squared distances of the dual quasilattice sites from their center of mass. Up to a factor N it is equal to the variance in the orthogonal space (see Sec. III A). The precise definition of the energy of the configuration α is

$$E^{(\alpha)} = C \left| \sum_{j=1}^N \left| \mathbf{y}_j^{(\alpha)} - \frac{1}{N} \sum_{i=1}^N \mathbf{y}_i^{(\alpha)} \right|^2 - \sum_{j=1}^N \left| \mathbf{y}_j^{(0)} - \frac{1}{N} \sum_{i=1}^N \mathbf{y}_i^{(0)} \right|^2 \right| . \quad (4)$$

The index 0 denotes the ideal reference configuration, $C = \frac{250}{61}$ is an arbitrary normalization constant.

This energy measure is called the **harmonic energy measure**. The variance for the ideal reference configuration 0 is smaller than the variances for the overwhelming majority of the random tiling configurations α . But there is a tiny minority of configurations with a variance smaller than the value of the ideal tiling. Their atomic hypersurfaces are closer to a sphere than the triacontahedron. Such configurations may play a rôle at very low temperatures. To avoid energies less than the energy of the ideal tiling we have taken the absolute value in Eq. 4. For zero global phason strain in an ideal tiling this energy measure is not degenerate. But for periodic approximants the N possibilities (N : number of lattice points) to chose the origin of the unit cell yield a ground state entropy $s_0 = \frac{\ln N}{N}$ per lattice point. It is obvious that s_0 vanishes in the thermodynamic limit. Strandburg [3] has introduced a similar energy measure. But it was taken relative to a fixed point in the orthogonal space and not relative to the center of mass and therefore does not fulfil the criterium of finiteness of the energy measure (third condition). Without fixed boundaries of the system the whole distribution of the dual quasilattice points in the orthogonal space may drift and therefore yield a systematic contribution to the energy.

Other global energy measures (not limited!) which we have used on a trial basis are the **cubic energy measure**

$$E^{(\alpha)} = \sum_{j=1}^N \left| \mathbf{y}_j^{(\alpha)} - \mathbf{M}_{Tria} \right|^3$$

and the **quadratic energy measure**

$$E^{(\alpha)} = \sum_{j=1}^N \left| \mathbf{y}_j^{(\alpha)} - \mathbf{M}_{Tria} \right|^2$$

(the latter one has been introduced by Strandburg [3]). \mathbf{M}_{Tria} denotes the fixed center of mass of the triacontahedron in the orthogonal space.

An example of a locally defined energy measure is the one that counts the violations of the alternation condition. This condition requires that along a worm two rhombohedra of the same type and orientation do not occur subsequently. This energy measure was used by Dotera and Steinhardt [6] and Gähler [11]. Other examples are the “simple energy model” which assigns the same energy to each forbidden verte, the “cluster energy model” which maximizes the frequency of certain favourite vertices and the “Tübinger mean-field model”. All three where used by Joseph in [10].

C. Pair interactions

All energy measures discussed in Sec. IV B contain a certain kind of arbitrariness since they do not depend on interatomic interactions but on the assignment of an increased energy value to randomized lattice configurations. Here we present test interactions which are motivated by pairwise interactions between atoms sitting on certain sites of the quasilattice (called “decoration”). We test whether the energetic equidistribution postulated in the random tiling model is justifiable.

The potential interactions used are the 12-6-Lennard-Jones potential modified by a cutoff function to guarantee a smooth behaviour at the cutoff radius ($r_c = 4$ in units of rhombohedra edges). Another model is the potential of mean force

$$v(r) = -\ln(g(r) + \kappa), \quad \kappa > 0.$$

$g(r)$ is the radial density function and κ an arbitrary parameter which screens the singularity caused by the zeros of $g(r)$ ($\kappa = 100$ in this work). To arrive at a potential which does not consist of purely delta-like minima due to the delta-like maxima of $g(r)$ of an ideal quasicrystal one usually broadens the maxima with a gaussian. This yields an additional free parameter, the width (if all the maxima are broadened by the same function).

The results of the test are presented in Sec. VIII C 1. It turns out that different random tiling samples are indeed equivalent with respect to the pair interactions, since the radial distribution function is nearly unchanged for the short distances (where the contribution to the potential energy would be strong), and at larger distances the pair potential is zero due to the cutoff distance.

V. CONSTRUCTION OF RANDOM TILINGS

A. Monte-Carlo method

Simpleton flips directed in their frequency by the Monte-Carlo method allow the generation of equilibrium configurations at a given temperature. The randomization of the quasilattice is realized by a sequence of such flips which usually are associated with a change in energy. The flips play the role of elementary transition paths between different states of a system in contact with a heat bath.

We are assuming that the method is ergodic [21]. Although this has not yet been proven, there is no hint up to now of the opposite. The method has already been used extensively to generate and study equilibrium random tiling quasicrystals. It is the only one known that produces equilibrium ensembles.

A simpleton flip does not generate or destroy tiles, it only rearranges them. Therefore the frequency of both types of rhombohedra in the tiling is remaining constant. The average orientation of the hypersurface and the global phason strain are not changed.

During the Monte-Carlo simulation lattice points are selected at random. If a lattice point belonging to the simpleton vertex is hit, the energy of the original and the flipped configuration are compared. If the energy decreases, the flip is always carried out. If it increases, it is performed with a probability of $\exp(-\frac{\Delta E}{k_B T})$.

During the flips the lattice points change their positions and the vertices their frequency. The simpleton vertex itself, for example, occurs with a frequency of 23.61% in the ideal tiling. This value decreases to a temperature dependent equilibrium value during the initial phase of a simulation. At $T = \infty$ the equilibrium frequency of the simpleton vertex is about 17.5%.

B. Boundary conditions

Quasicrystals do not permit periodic boundary conditions. Hence one has to work with a finite patch of a quasicrystal. Then there are two possibilities to deal with the surface: either keep it fixed (fixed boundaries) or identify opposite sides (periodic approximants).

In the case of fixed boundaries the surface lattice points are not allowed to move. In approximants all lattice points are mobile. Therefore the configuration entropy per lattice point with fixed boundaries is smaller than the entropy of approximants. The configuration entropy of the approximant, on the other hand, differs only slightly from the value of the ideal tiling. The frequency of vertices also is not much different between an ideal quasicrystal and an approximant tiling. The frequency of the simpleton, however, in patches with fixed boundaries may grow to up to 30% of that of the bulk vertices. For a discussion of the entropy dependence on boundary conditions see [22].

Periodic approximants show matching rule violations already in the ground state. They exhibit a periodic superstructure and for very small samples a remarkable deviation of the vertex frequencies. The intrinsic global phason strain changes the flip diffusion properties at low temperatures as the ground state phasons generate zero energy modes. The sheet magnetization (see Sec. III C) in the case of a cubic approximant is useful only for the three two-fold directions parallel to the cubic cell axis. The acceptance region is no longer densely covered but has a lattice structure. This fact causes problems in the averaging procedures described in Sec. III E.

C. Addition method

A new method to generate random tilings (especially non-equilibrium configurations) is the successive addition of tiles to the tube and slab structures within a finite region.

For this method fixed boundaries are used. We start with a patch of a tiling with a fixed (possibly zero) global phason strain. This can be e.g. a piece of an ideal tiling or a single unit cell of a periodic approximant. All interior quasilattice points are removed. Then the volume is refilled in a systematic way without gaps and overlaps of the tiles. Since we start with an existing patch (microstate), it is certain that tilings of this surface must exist. The hollow volume represents the macrostate, the different possibilities to fill it are the microstates.

The algorithm is started by selecting one five-fold direction (Fig. 5). First the ensemble of parallel slabs perpendicular to this direction has to be filled with rhombohedra. The borders of the slabs are given by a surface consisting of rhombi parallel to the five-fold axis chosen. A slab appears as a pentagonal Penrose rhombus pattern in projection.

The surface of the hollow volume and the correlation between the slabs dictate the addition conditions. A violation sooner or later leads to gaps or overlaps, and the configuration has to be abandoned.

We will now shortly sketch how the method works. The procedure can be broken up into two parts: filling the two-dimensional slabs, which is equivalent to performing the construction for generalized Penrose tilings, and then filling the space between the slabs.

First of all we will explain how to proceed in two dimensions. In the Penrose tiling there are five sets of one-dimensional rows of rhombi with one type of edge in common. The average direction of the sets is perpendicular to the tiling vector directions. In the hollow volume we start with one of the directions and generate the rows one by one. The fixed surface determines the starting and terminating position of the rows (by the edges parallel to the selected tiling vector). The difference vector (in higher dimensional coordinates) between initial and final point determines the number of tiles of each type in that row uniquely (by the coordinate components). We are only free to choose the sequential arrangement of the tiles. There are, however, restrictions: The second pair of edges of each rhombus must also fit into the configuration. This means that the difference vector between the rhombus and the respective edge on the surface of a neighbouring row must be fillable with rhombi. Otherwise, the configuration has to be abolished. After all the rows of

one direction have been created, the next direction is being dealt with until the whole patch is filled. The last direction is redundant, since the whole slab is filled as soon as the second-to-last direction is worked out.

Up to a certain degree the process is running analogously in the three dimensional case. The slabs are being filled in the same way as for twodimensional Penrose-like rhombus tilings. We continue with the next slab perpendicular to the selected five-fold direction and generate slab by slab along this direction. Now we have to check the difference vectors of two pairs of edges to make sure that the space in between can be filled. But one must be careful as there are row directions crooked by oriented with respect to the row directions within each slab. For example, the row direction perpendicular to the rhombus spanned by the vectors t_2 and t_3 are crooked with respect to the corresponding direction of the vectors t_0 and t_1 . To explain how to overcome this problem, however, takes more space than is available here. Interested readers are referred to [23]. After all slabs of one direction are constructed the other directions are attacked until the whole volume is filled. Tilings generated by this method are called “addition tilings”.

D. Comparison of the methods

The acceptance domain for the ideal icosahedral rhombohedral tiling is a triacontahedron (Fig. 6). In an equilibrium configuration generated by the simpleton flip method it is smeared out to an almost Gaussian distribution. Differences in the physical space are relatively small. There are some matching rule violations like pairs of adjacent rhombi of the same type, but the structure does not appear to be massively disordered. The phason fluctuations of the configurations are limited according to [2].

In a configuration generated by the addition method the deviation from quasiperiodicity is much stronger (Fig. 6): There are microcrystalline inclusions which indicate large-wavelength fluctuations in the higher-dimensional space. Many twin, domainlike or grain boundaries occur. The deviation from the ideal acceptance domain is strong and anisotropic. Configurations far from equilibrium are easy to construct.

The efficiency of a specific method depends on its ergodicity properties. In a configuration generated by the addition method with microcrystalline inclusions there are few possibilities for flips. Very often the few flippable lattice points only jump back and forth. There are bottle necks which prevent or strongly inhibit the structure from moving through phase space.

Furthermore a configuration depends on its history. To generate independent configurations one has to wait until the autocorrelation is dropped off sufficiently. At high enough temperatures about 50 Monte-Carlo steps are sufficient. Fixed boundaries may increase the correlation times drastically.

The anisotropic character of the configurations generated by the addition method is due to the fact that the slabs are filled sequentially. The deviation of the center of mass of the point distribution from the original acceptance domain depends on the sequence of construction of the slab and tube directions. On the other hand, it is only the sequential treatment that permits the tractability of the method.

In the addition method the probabilities for adding a certain rhombohedron at a certain place have not been taken into account. Therefore, the configurations generated by this method in a selected hollow volume can not be considered as the sample survey of a equilibrium ensemble. To calculate the probabilities would be impossible since the number of realizations is prohibitively high.

The addition method allows the generation of configurations that are never reached in acceptable times by the simpleton flip process. The method could be used to generate random tilings with constraints.

Experimentally, a number of decagonal quasicrystals have been found that maybe could be described by configurations generated by the addition method [24–27]. The distribution of the

quasilattice points in the orthogonal space is not isotropic as in the samples produced by the simpleton method but strongly anisotropic.

VI. RANDOM TILING TRANSITION AND STRUCTURE FUNCTIONS

Signals for a random tiling transition can be obtained in a number of ways. The thermodynamic functions u , c_V and s may show a characteristic behaviour. For example a plot of the specific heat c_V versus temperature for different sample sizes (finite-size scaling) may indicate the possibility of a random tiling transition. The specific heat c_V should diverge in case of a second order phase transition.

For any desired temperature a histogram of frequency of the energy values can be calculated during the simulation. The histogram for infinite temperature yields an approximation for the density of energy states since at infinite temperatures all energy levels should be occupied with equal probability. Therefore it may be used to explain the behaviour of the specific heat as a function of T (see also Sec. VIII B 1).

In addition to the specific characterization criteria for quasicrystals described in Sec. III there are more general functions that can indicate a phase transition. We have applied the following:

1. Self diffusion coefficient

The average squared difference $\langle (\mathbf{r}(t) - \mathbf{r}(0))^2 \rangle$ of the coordinates of all quasilattice points from their initial position is expected to depend linearly on time at long enough simulation times. The slope of the function is proportional to the self-diffusion coefficient D . A change of the slope may indicate a phase transition which involves the change of energy barriers for example.

2. The Binder order parameter

The Binder order parameter [28] $B^{(N)}(T)$ for a given sample size N and temperature T is defined by

$$B^{(N)}(T) := 1 - \frac{M_4^{(N)}(T)}{3 \left(M_2^{(N)}(T) \right)^2}$$

where $M_2^{(N)}(T)$ and $M_4^{(N)}(T)$ are the second and fourth moment

$$M_k^{(N)}(T) = \int d\mu \left(p(\mu)^{(N)}(T) \right) \mu^k$$

of the probability $p(\mu)$ of a microstate of the sheet magnetization μ belonging to a macrostate with sheet magnetization M . The Binder order parameter $B^{(N)}(T)$ is plotted as a function of T and yields a set of curves parametrized by N . A unique intersection point of the curves points to a second order phase transition and yields the transition temperature. If there is no clear intersection point only an interval for a possible phase transition can be determined.

A. Structure functions

1. Radial distribution function $G(r)$

The radial distribution function $G(r)$ of lattice points or atoms (in case of a decorated quasilattice) consists of discrete delta-type maxima and is related to the radial density function $g(r)$ by $G(r) = 4\pi r^2 g(r)$. The Fourier transform of the radially averaged $G(r)$ is the radial structure factor $I(k)$. The potential energy u of an quasicrystal can be directly calculated from $G(r)$ if there are only pair interactions $v(r)$:

$$u = \sum_{r=0}^R G(r)v(r) \quad (5)$$

where R is the cutoff radius of the potential. If there are different types of atoms, then additional sums over the different types of interaction pairs must be taken.

2. Structure factor intensity $I(k)$

Flips of the tiles modify the occupation density of atomic chains and atomic layers. Diffraction diagrams are dominated by the long-range translational and orientational ordering of quasicrystals. Therefore an alterations of the quasiperiodicity changes the width and intensity of reflexions.

Phason fluctuations furthermore generate diffuse scattering. Due to the limitation of the phason fluctuations [2] the maximal intensities are barely influenced. Diffuse scattering is governed by the phason-elastic constants.

3. Diffraction diagrams

Diffraction diagrams for random tilings were calculated for randomly selected sample configurations filed during the simulation process at a given temperature T and size N and averaged over the whole set chosen. The fluctuations between the selected configurations turned out to be small at a given T and N .

VII. SIMULATION PROCESS AND MODELS STUDIED

The internal energy u , the specific heat c_V , the entropy s as well as the sheet magnetization M , the corresponding susceptibility χ and the self-diffusion coefficient D , all dependent on the temperature T , are thermodynamical state variables of a random tiling ensemble. The structure of a single tiling, but also the whole ensemble can be characterized by structural functions. In this work we have used the diffraction-intensity $I(k)$ (without paying attention to diffuse line shapes), the relative frequencies of vertex environments, the axial and planar structures, the variance Ω (phason fluctuations) and the radial distribution function $G(r)$. The quantities u , M , Ω and $\langle (\mathbf{r}(t) - \mathbf{r}(0))^2 \rangle^2$ are sampled by registering their values at regular intervals of length Δt during the simulation. From the collected data all above mentioned state variables are calculated. Data of microconfigurations are stored every $1000 \cdot \Delta t$ Monte-Carlo step. The results may deviate from the thermodynamical limit due to finite-size-effects. If the sample size grows, the values should converge to the thermodynamic limit.

An initial configuration (e.g. an ideal Ammann-Kramer-Penrose approximant or an addition configuration) was equilibrated over a typical thermalization time of 10^3 to 10^4 steps before the real

²The simulation time is set to zero after thermalization.

simulation was started. The thermalization time was chosen according to the saturation behavior of the energy, for example. At low temperatures longer equilibration and simulation times and sampling intervals were used. The length Δt was checked by the decay of the autocorrelation functions. For high temperatures Δt was set typically about 50 Monte-Carlo moves per lattice point, while for lower temperatures 200 moves were taken due to temporal correlations. The entire duration of a simulation run at given temperature typically has been about $25000 \cdot \Delta t$ to $30000 \cdot \Delta t$ simulation steps.

A. System sizes and interaction types

The following systems have been studied in our simulations:

1. A finite patch of a quasiperiodic lattice with 4403 lattice points (3507 cells), fixed boundaries and the cubic energy measure. Starting configuration has been the ideal quasilattice.
2. A cubic approximant with 2440 lattice points, periodic boundaries and the quadratic energy measure. Starting configuration was the ideal approximant.
3. Two five-fold approximants with 890 and 1440 lattice points, periodic boundaries and the harmonic energy measure. Starting configuration also has been the ideal approximant.
4. Five cubic approximants with 136/712 (n=3), 576/3016 (n=4), 2440/12776 (n=5), 10336/54120 (n=6) and 43784/229256 (n=7) lattice points/atoms in the binary decoration model³ [29] (n is the generation), periodic boundaries and the harmonic energy measure. In this category we used ideal approximants as well as addition tilings as starting configurations. Here we also calculated the self-diffusion coefficient $D(T)$, the magnetization $M(T)$ and the susceptibility $\chi(T)$. The results are independent of the starting condition in the case of periodic boundaries: Ideal quasicrystals and addition tilings yield the same ensemble averages⁴, proving that the system had been well equilibrated before data collection.

VIII. RESULTS

A. Direct calculation of the configurational entropy

For small clusters of rhombohedra with fixed surface it is possible to calculate the configurational entropy s directly, which we have performed for the five smallest polyhedra with triacontahedral shape and edge lengths of one or two. The results are presented in Tab. I.

The clusters are too small to permit a reasonable extrapolation to the thermodynamic limit. The value of the entropy is also too small due to the fixed boundaries.

B. Thermodynamic functions

³In the binary model each vertex and edge center is decorated with a small atom, and the long diagonal of the prolate rhombohedron is decorated with two large atoms

⁴which is not true in the case of fixed boundaries

1. Internal energy, specific heat, entropy

In sample one the ground state entropy vanishes. The internal energy grows with T and saturates at high T . Due the fixed boundaries the saturation limit is finite although the energy measure is unlimited. The specific heat grows until $T \approx 1$. Then it decreases and goes to zero at high T i. e. we observe a SCHOTTKY anomaly as is typical for two level systems. The entropy at infinite temperature approaches $s_\infty \approx 0.1194 \pm 0.015$.

Sample two behaves similar, but the saturation of the internal energy for $T > 10$ is not so clearly visible and may indeed not occur since the energy measure is not limited and periodic boundaries were applied in this case. The decay of the specific heat is slower which is also a consequence of the energy measure. The entropy at infinite temperature approaches $s_\infty \approx 0.2621 \pm 0.015$.

Samples three and four are again quite similar. The internal energy grows monotonously, and a clear saturation becomes visible (Fig. 7). The saturation value of u depends on the size of the sample. The limit value can be derived from limits of the variance: $\Omega(T=\infty) = 1.73 \pm 0.01$ [2] leads to u between 1.97 and 2.05. A SCHOTTKY anomaly in the c_V -Plot again is present but the specific heat shows an additional bump above the maximum (Fig.8). Such a behaviour is known for few-level systems (for example three-level systems) with sufficiently separated levels. We have mapped the distribution of the energy levels for $T=\infty$. No indication of discrete energy levels was found, only an asymmetry of the distribution with a smaller slope at higher energies could be observed. There are other energy measures [11] which exhibit no visible asymmetry in the energy distribution and no bump in the specific heat. This, however, is in our opinion not a clear explanation for the phenomenon. The value of the maximum of c_V is not significantly dependent on sample size. The increase in s_∞ is caused only by the growing width of maximum (Fig. 9). Entropy values at $T = \infty$ are listed in Tab. II. Since no divergence occurs with increasing sample size, we have no hint for a second order phase transition.

2. Simpleton magnetization, simpleton susceptibility, Binder order parameter

The temperature dependence of the energy fluctuations and the specific heat do not give a clear indication for a phase transition. There is no divergence of the maximum of c_V . The reason may be that the intrinsic divergence of the specific heat with sample size, if any, is very weak. For further insight we calculated the sheet magnetization M and the susceptibility χ since the latter shows a much more pronounced divergence behaviour.

In the samples of class four the magnetization saturates at high T , and the minimum value decreases with size (Fig. 10). At higher temperatures, between $T = 3$ and 10, it increases again. This behavior we attribute to the finite size of the samples. The value of the maximum of the susceptibility grows almost linearly with the generation n and moves to lower T (Fig. 11). It is not yet clear if the relation $\chi_{max}(n) \propto (n - n_0)$ is valid for $n > 7$. If yes, this would be a slow divergence (more precisely: $\chi_{max}(N)$ is about proportional to $\tau^3 \sqrt{N}$ where N is the number of lattice cells and $\tau = \frac{\sqrt{5} + 1}{2}$). With our current simulation programs it is not possible to deal with $n \geq 8$.

The Binder order parameter does not lead to a decision either, since there is no clear intersection point visible (Fig. 12). The trend of $B^{(N)}(T)$ changes at $n = 5$, similar to the magnetization behaviour. The most probable intersection point is between $T = 0.3$ and 0.4 if it exists.

But the tendency of χ_{max} with n and the behaviour of $B^{(N)}(T)$ indicate that a phase transition is much more likely to occur at $T = 0$.

3. Self-diffusion coefficient

The mean square displacement $\langle (\mathbf{r}(t) - \mathbf{r}(0))^2 \rangle$ grows linearly with time t , indicating a normal diffusion behaviour and allowing the calculation of the diffusion coefficient D . At temperatures lower than $T \approx 1$ the extrapolation is difficult due to large fluctuations. D becomes unmeasurably small below $T = 0.5$. The diffusion coefficient forms a plateau at $T \gtrsim 1$ for $n = 4, 5, 6$ in the ARRHENIUS plot (Fig. 13). There may be several reasons for this behaviour:

First, there are energy barriers between different tiling configurations due to the harmonic energy measure, which at low temperatures lower the mobility of lattice points for flips of higher energy. In the range of the plateau the probability for a flip only occasionally suffices to overcome the barriers which play no role at high temperatures.

Second, a phase transition may occur which changes the slope in the ARRHENIUS plot. Gähler has also observed a change of the slope in case of the energy measure with the alternation condition which turns out to be a phase transition since other response functions like the susceptibility and the specific heat definitely yielded a divergence at the same temperature.

Last, there is an explanation which comes from the fact that the number of flippable lattice points (number of simpletons) changes with temperature. We can distinguish four ranges:

1. The number of simpletons is about 23% in the range $0 \leq T \lesssim 1$.
2. In the range $1 \lesssim T \lesssim 10$ we find a nearly logarithmic decrease of the number of simpletons. The plateau of $D(T)$ is clearly seen here.
3. In the range $10 \lesssim T \lesssim 100$ the approach of the frequency of the simpleton to a constant value leads to an increase of the negative slope of $D(T)$.
4. Above $T \gtrsim 100$ the number of simpletons is constant at $\approx 17.5\%$.

In the approximants the behaviour of $D(T)$ is obscured to some degree by zero energy modes caused by periodic boundaries. These modes become less and less important at larger sizes, but suppress the plateau for small sample sizes.

Within the framework of the random tiling model we have studied only flip diffusion. No other diffusion mechanism, in particular vacancy diffusion, can be introduced in this way. The latter mechanism is expected to be the dominant diffusion process at least above 600°C, but there are indications that the new mechanism plays a rôle below that temperature [30].

C. Structure functions

1. Radial density function, radial structure factor, pair interaction energy

Structure functions have been calculated for samples of type four and size $n = 6$, containing 10336 lattice points, for the primitive monoatomic and the binary decoration [29]. There are only small changes in the radial density function $g(r)$. The largest differences of the order of 12% occur for bonds between two large atoms, but they are the least significant ones for stability due to their small number. The energetically most important nearest-neighbour bonds change even less in all cases, since a large portion of them lives *within* the rhombohedra and thus is only transferred to another position by a flip, but the frequency itself does not change. The differences we observe in the addition tiling are somewhat larger, but still very small. Figure 14 shows the results for a monatomic sample of size $n = 5$.

The trend of the radial structure factor $I(k)$ which corresponds to the FOURIER-transformation of $g(r)$ is similar to that of the radial density function. Due the smallness of the sample there are rather large finite size effects which do not permit a quantitative comparison.

We further observe a very small dependence of the pair energy function (see Eq. 5) on size and T due to the relation between the pair energy and the pair distribution function. It is interesting

to note that the potential energy of the random tiling ensemble is at $T = \infty$ about 0.4% lower than for the ideal quasicrystal for a large class of LENNARD-JONES-like potentials, whereas the fluctuations within the random tiling ensemble are of the order of 0.1%. Therefore simple pair potentials obviously favour energetical equidistribution, i. e. the random tiling model.

2. Variance, vertex statistics

The variance behaves roughly linear with respect to u which is obvious if one compares their definition in Eqs. 1 and 4. The variance therefore shows a similar behaviour as the internal energy.

The change in the statistics of the vertices with temperature is much more important, as we have seen in the discussion of the diffusion behaviour and in the rôle of the simpleton frequency in Sec VIII B 3. The changes of the vertex frequencies (Notation as in [31]) can be summed up as follows:

1. The simpleton vertex 1 (452)⁵ decreases from 23.61% to 17.5%.
2. Vertex 3 (670) decreases from 23.61 % to less than 10%.
3. Vertex 2 (561) increases from 23.61 % to 29 % at $T = 8$ and then decreases to 26%.
4. The sum of frequencies of vertex 1 and vertex 2 is roughly constant.
5. The forbidden vertices (all together) increase from 0% to more then 40%.
6. The vertex with the highest symmetry where 20 prolate rhombohedra meet (vertex 24, in [31] also called twelve-fold sites) decreases in frequency from 1.2% close to extinction.

The addition tilings show a strong deviation from the ideal distribution. For the sizes $n = 4, 5, 6$ we obtain for the simpleton frequencies: 16.7 %, 15.0 %, 12.2 %, and for the frequencies of the forbidden vertices: 36.3 %, 43.2 % and 55.3%, respectively.

We note that the statistical error of the vertex statistic is — in the case of equilibrium random tilings — largely independent of the sample size and already for $n \geq 4$ very small.

3. Plane and axial structures

Plane and axial structures have been calculated for a sample of type four with the size $n = 6$, containing 10336 lattice points. The area function $A_s(\xi^\perp)$ has been calculated from the dual lattice points in the orthogonal space, and the histogram of the densities $H(\rho_F)$ has been derived by numerical differentiation as described in Sec. IIID. The analysis has been carried out at temperatures $T = 0.3, 1, 3, \dots, 1000$ for planes perpendicular to two-, three- and fivefold planes.

There is a continuous transition from an area function $A_s(\xi^\perp)$ which is dependent on the symmetry directions to an almost isotropic gaussian shape at high temperature, indicating that the acceptance domain is smeared out isotropically. At $T = \infty$ the histogram of densities $H(\rho_F)$ also becomes almost independent of the symmetry direction. $H(\rho_F)$ is strongly peaked at very low and very high plane densities which indicates that very weakly and very densely occupied planes dominate.

⁵The first digit is the number of vertices connected by an edge, the second the number of vertices connected by a short face diagonal and the last the number of atoms connected by a short diagonal of the oblate rhombohedron

In the five-fold direction we observe the smallest changes. Strong differences between the analytical and numerical functions, especially at poles and singularities, for three- and two-fold directions prohibit quantitative predictions.

The addition tilings show a broader distribution in $A_s(\xi^\perp)$ and an anisotropy. Additional minor maxima occur in $H(\rho_F)$, but they alternate from one realization to the other. The distribution of dual lattice points of one tiling is anisotropic by construction. To obtain $A_s(\xi^\perp)$ we have averaged over all symmetry-equivalent directions.

We could not find any useful results for axial structures. The size of the samples appears to be too small to give a satisfying resolution for histograms. Strong differences between analytical and numerical $H(\rho_l)$ functions for $T=0$ also indicate that the results are not reliable.

4. Diffraction patterns

Diffraction patterns (Bragg scattering without observation of diffuse line shapes which are characteristic for random tilings) have been calculated for a sample of type four with the size $n = 5$, containing 2440 lattice points. The analysis has been carried out at temperatures $T = 0, 0.3, 1, 3, 10$, and at $T = 10000$ for planes perpendicular to two-, three- and fivefold planes. The intensities are only weakly dependent on temperature as the acceptance domain is only weakly smeared out even at high temperatures. This result is consistent with Tang's observation of limited phason fluctuations in three dimensions [2].

In the case of the addition tilings stronger differences exist: Some of the reflexions are weaker, and new ones arise. This indicates that there is already a large phasonic disorder in the addition tilings which generates an extended cloud of dual lattice points.

IX. CONCLUSIONS

We have investigated a geometric and thermodynamic model of disordered quasilattices, which could explain the structure of icosahedral metal alloys.

In this random tiling model there are no matching rules, in contrast to the ordered quasiperiodic structures. The only requirement is that the physical space must be filled with rigid tiles without gaps or overlaps.

The results are summarized as follows:

1. The internal energy u increases and saturates at high temperatures. u_∞ converges towards a limit for $N \rightarrow \infty$, which can be estimated from values of the phason fluctuation variance for the pure entropic random tiling ensemble. The entropy s_∞ obtained from the specific heat c_V by thermodynamic integration is about 0.24 ± 0.01 , in agreement with results from many other sources [3,9,11]. The specific heat c_V shows a SCHOTTKY anomaly. It is not clear whether it diverges. The increase of the entropy with the system size comes from the broadening of the maximum.
2. The sheet magnetization decreases to a minimum with the temperature and slightly grows to a saturation value. In the thermodynamic limit it should vanish without an intermediate minimum. The susceptibility diverges slowly, the maximum shifts to smaller temperatures. The Binder order parameter does not exhibit a unique intersection point. We assume that the transition temperature is finite, hence the random tiling transition could be analogous to the transition in a two-dimensional Ising ferromagnet.
3. The self-diffusion coefficient displays a plateau in the central temperature range indicating energy barriers for certain flips due to the harmonic energy measure. On the other hand there exist correlations between the temperature dependence of the self-diffusion coefficient and the frequencies of simpletons per lattice point. The Arrhenius plot is deviating strongly from

that assumed by Kalugin and Katz [7]: Where these authors are plotting a steep increase, we are observing the plateau. There are zero energy modes due to periodic boundary conditions, which lead to a suppression of the plateau for small approximants.

4. Henleys postulate of the finiteness of the phason fluctuations is demonstrated by the Monte-Carlo-simpleton-flip tilings. The addition tilings show larger variances and deviations of the vertex frequencies from the equilibrium values. There are also changes in the diffraction patterns caused by phason fluctuations.
5. The frequencies of the densities of planes in the equilibrium tilings are temperature dependent and very weakly and very densely decorated planes dominate. Addition tilings show further minor maxima, dependent on the realization.
6. Radial structure functions depend only weakly on the configuration. This is due to the rigidness of the cells. Pair interactions realize an equidistribution of all configurations — a possible realization of the pure entropic random tiling model.

The behaviour of c_V and χ obviously depends strongly on the type of energy measure used. The alternation condition seems to work much better [11] — maybe as consequence of its closer similarity with Ising interaction models in comparison with the harmonic energy measure. However, for the simple energy model [10] it was also not possible to decide if a phase transition occurs, since no divergence of the specific heat could be observed.

ACKNOWLEDGEMENTS

The authors are very indebted to Franz Gähler for helpful discussions.

[1] V. Elser, Phys. Rev. Lett. **54** (1985) 1730.
[2] L. H. Tang, Phys. Rev. Lett. **64** (1990) 2390.
[3] K. J. Strandburg, Phys. Rev. **B44** (1991) 4644.
[4] C. L. Henley, in *Quasicrystals - the state of the art*, Eds. D. P. DiVincenzo, P. J. Steinhardt, World Scientific, Singapore (1991) 429.
[5] W. Ebinger, Diploma thesis, Stuttgart (1991).
[6] T. Dotera, P. J. Steinhardt, Phys. Rev. Lett. **72** (1994) 1670.
[7] P. Kalugin, A. Katz, Europhys. Lett. **21** (1993) 921.
[8] E. Sørensen, M. V. Jarić, Phys. Rev. Lett. **73** (1994) 2464.
[9] M. V. Jarić, E. Sørensen, in *Proc. of the 5th Int. Conf. on Quasicrystals*, Eds. C. Janot, R. Mosseri, World Scientific, Singapore (1995) 363.
[10] D. Joseph, in *Proc. of the 5th Int. Conf. on Quasicrystals*, Eds. C. Janot, R. Mosseri, World Scientific, Singapore (1995) 605.
[11] F. Gähler, in *Proc. of the 5th Int. Conf. on Quasicrystals*, Eds. C. Janot, R. Mosseri, World Scientific, Singapore (1995) 236.
[12] N. G. de Bruijn, Kon. Akad. Wetensch. Proc. Ser. **A84**, (1981) 38.
[13] C. L. Henley, J. Phys. **A21** (1988) 1649.
[14] S. I. B. Abraham, Int. J. Mod. Phys. **7** (1993) 1415.
[15] A. Katz, M. Duneau, J. Physique **47** (1986) 181.
[16] T. Kupke, PHD, Stuttgart (1992).
[17] T. Kupke, H.-R. Trebin, J. Phys. I (France) **3** (1993) 1629.
[18] P. Gummelt, Geometriae Dedicata **62** (1996) 1.
[19] H. C. Jeong, P. J. Steinhardt, Nature **382** (1996) 431.

- [20] M. Baake, D. Joseph, Phys. Rev. **B42** (1990) 8091.
- [21] F. Gähler, private communication
- [22] D. Joseph, M. Baake, J. Phys. **A29** (1996) 6709.
- [23] W. Ebinger, PHD, Stuttgart (1996)
- [24] M. Hiraga, W. Sun, F. J. Lincoln, M. Kaneko, Y. Matsuo, Jpn J. Appl. Phys. **30** (1991) 2028.
- [25] Y. He, H. Chen, S. J. Poon, G. Shiflet, Phil. Mag. Lett. **64** (1991) 307.
- [26] M. Hiraga, F. J. Lincoln, W. Sun Mater. Trans. JIM **32** (1991) 308.
- [27] D. Joseph, S. Ritsch, C. Beeli, Phys. Rev. **B55** (1997) 8175.
- [28] K. Binder, D. W. Heermann, *Monte Carlo Simulations in Statistical Physics*, Springer, Heidelberg (1998).
- [29] J. Roth, R. Schilling, H.-R. Trebin, Phys. Rev. **B41** (1990) 2735.
- [30] R. Blüher, Diploma Thesis, Stuttgart (1997), R. Blüher, P. Scharwaechter, and W. Frank, in preparation
- [31] C. L. Henley, Phys. Rev. **B34** (1986) 697.

TABLE I. Configurational entropy for triacontahedral clusters with fixed surface. The first column codes the type of polyhedron by the length of edges in units of the six icosahedral basis vectors. The second column gives the number of configurations, the third the number of rhombohedra. The last column contains the configurational entropy per lattice point.

edge lengths	# configs.	# rhombo.	s
111111	160	20	0.2538
211111	1280	30	0.2385
112211	22381	44	0.2276
121121	22981	44	0.2282
221121	1268131	63	0.2231

TABLE II. Some thermodynamic parameters for the harmonic interaction model with periodic boundary conditions. The first column provides the generation for cubic approximants, the second column the number of lattice points, the following columns list the entropy s_∞ and the variance $\Omega(T=\infty)$. The rows “890” and “1440” denote pentagonal approximants.

n	size	s_∞	$\Omega(T=\infty)$
3	136	0.1816878	1.475 ± 0.015
4	576	0.2032964	1.56 ± 0.01
	890	0.2086351	1.60 ± 0.02
	1440	0.2076728	1.615 ± 0.02
5	2440	0.2114427	1.635 ± 0.01
6	10336	0.2349887	1.675 ± 0.01
7	43784	0.2367582	1.70 ± 0.01
	limit	0.24 \pm 0.01	1.73 ± 0.01

FIG. 1. Simpleton flip

FIG. 2. Worm of rhombohedra

FIG. 3. Plane structures in the ideal tiling. The left column contains the functions $A_s(\xi^\perp)$, the right column displays the histograms of plane densities $H(\rho_{F,s})$.

FIG. 4. Chain structures in the ideal tiling. The histograms of chain densities $H(\rho_{l,s})$ are given.

FIG. 5. Intermediate state in the addition process. The star indicates the tiling vector directions. The double arrow indicates the direction which has already been filled. The small arrows indicate the correlations to the direction which will be filled next.

FIG. 6. Comparison between different tilings: a) perfect quasicrystal, b) generated by flip process, c) generated by addition process. The corresponding acceptance domains are labeled by d), e) and f).

FIG. 7. Internal energy. Sizes are indicated by the number of lattice points.

FIG. 8. Specific heat. Sizes are indicated by the number of lattice points.

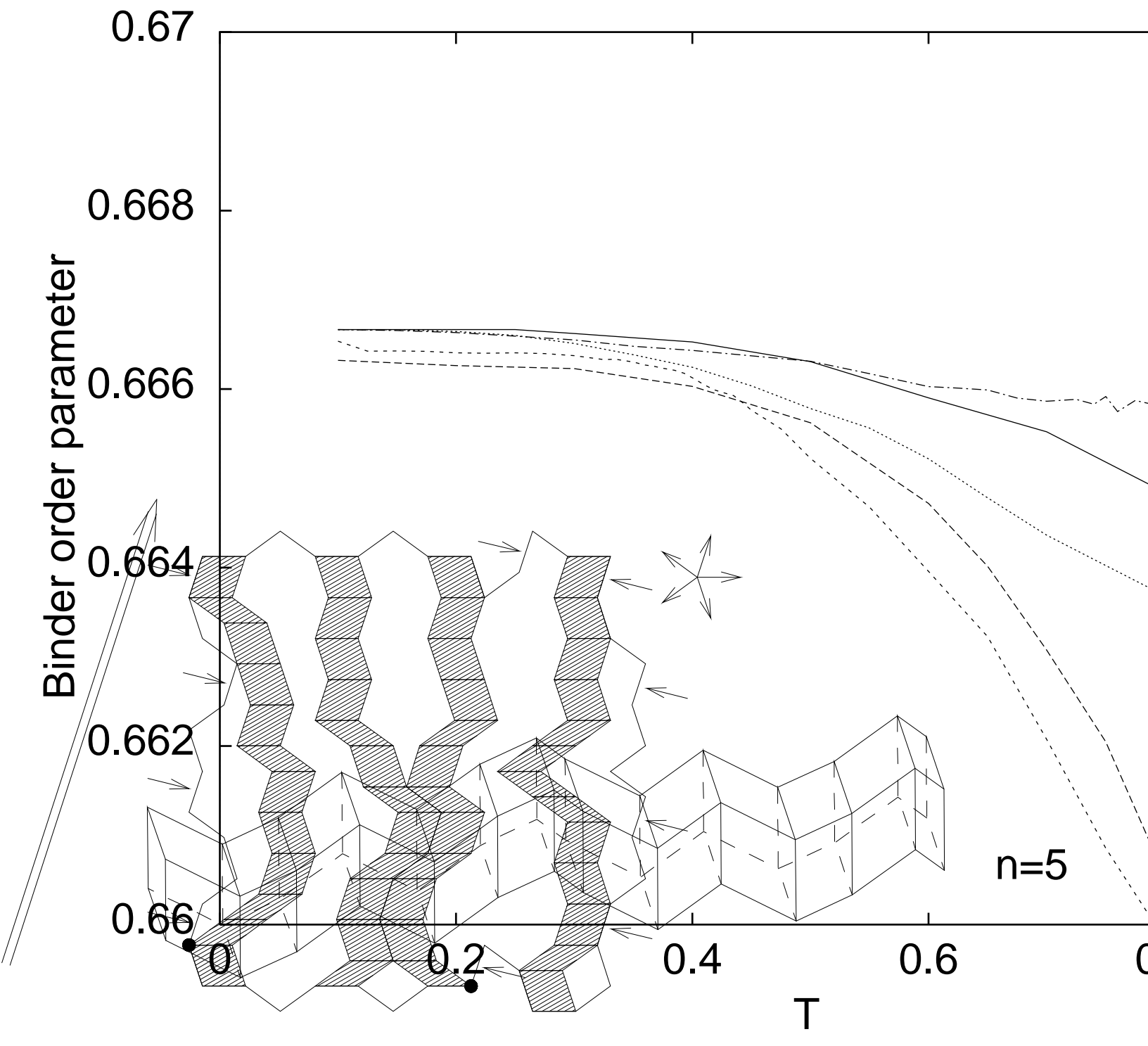
FIG. 9. Configurational entropy. Sizes are indicated by the number of lattice points.

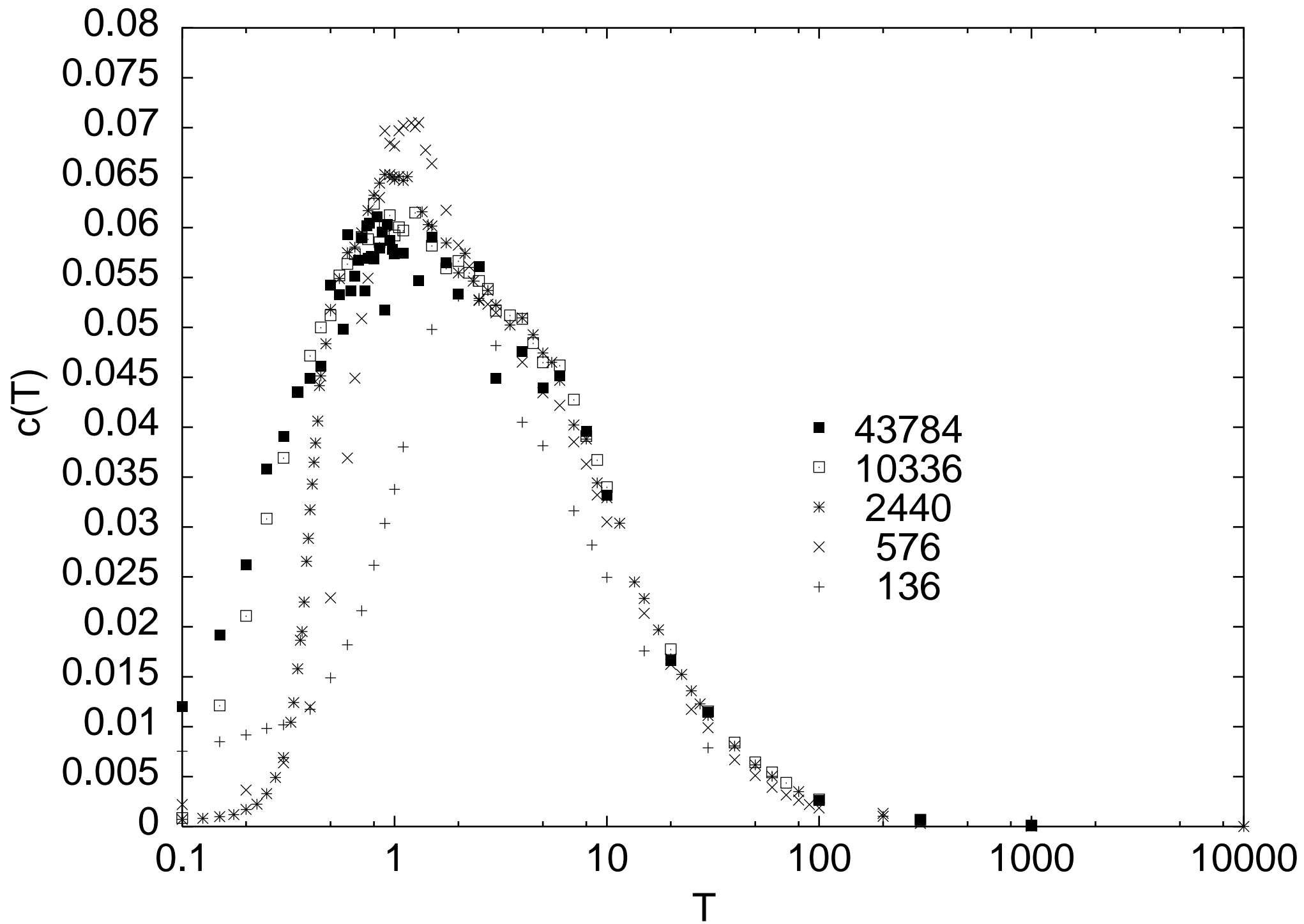
FIG. 10. Magnetization. Sizes are indicated by the number of lattice points.

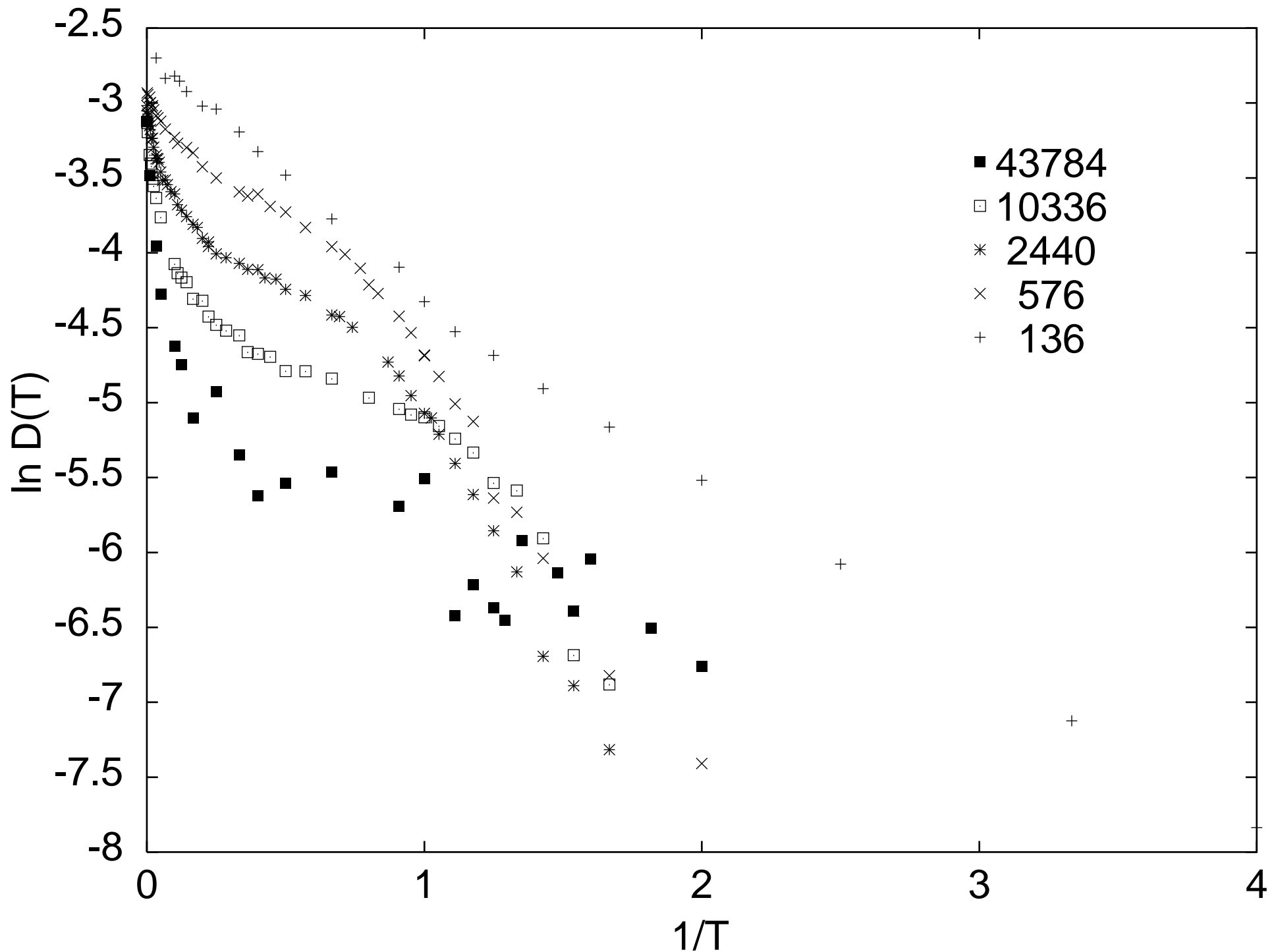
FIG. 11. Susceptibility. Sizes are indicated by the number of lattice points.

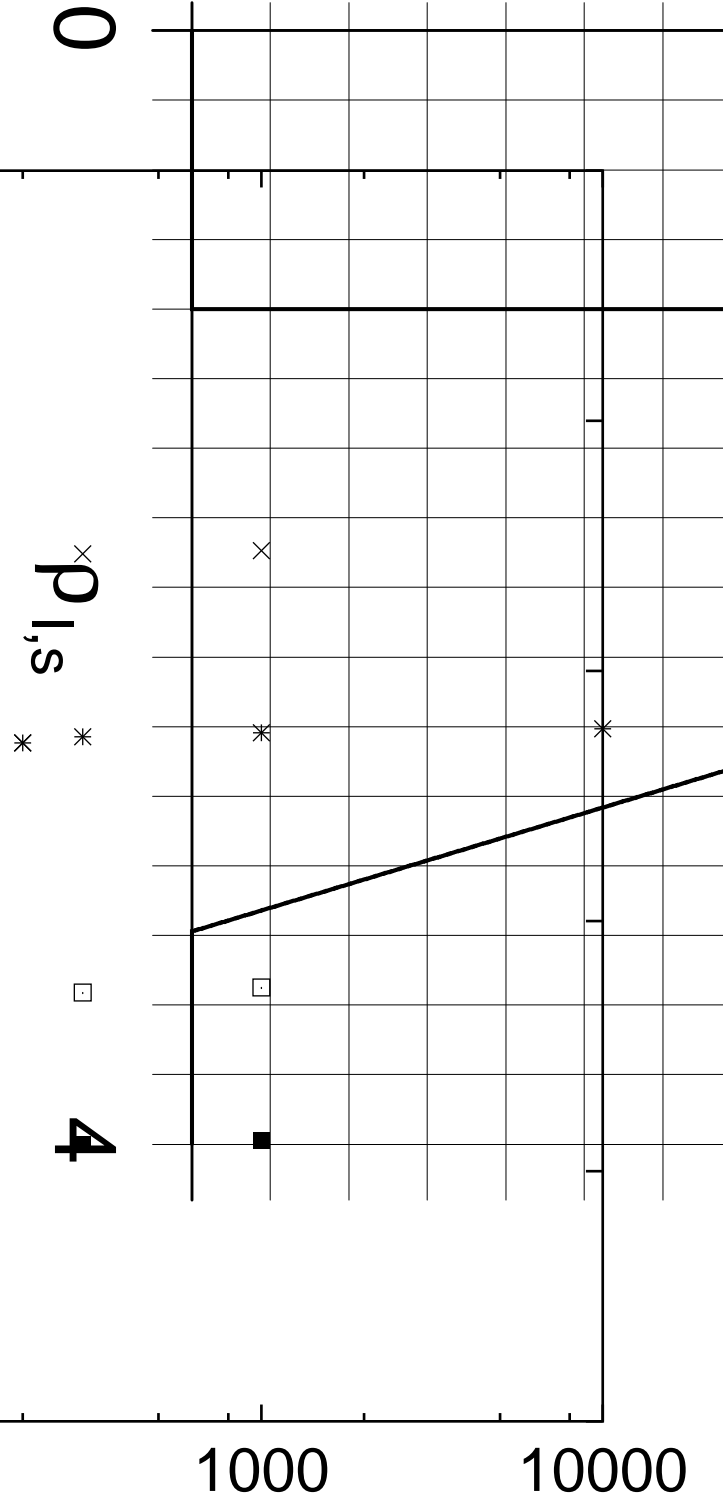
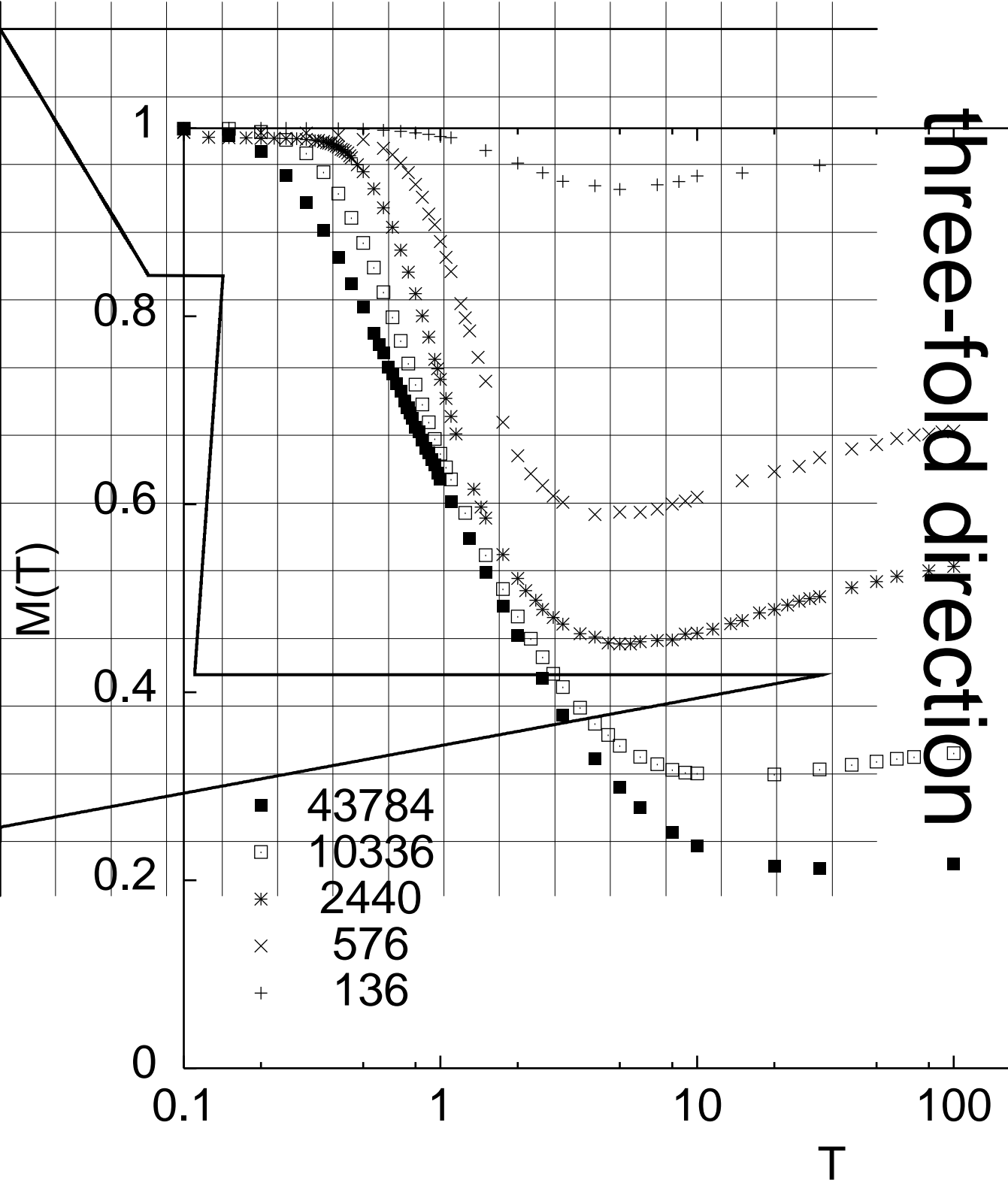
FIG. 13. Self-diffusion coefficient. Sizes are indicated by the number of lattice points.

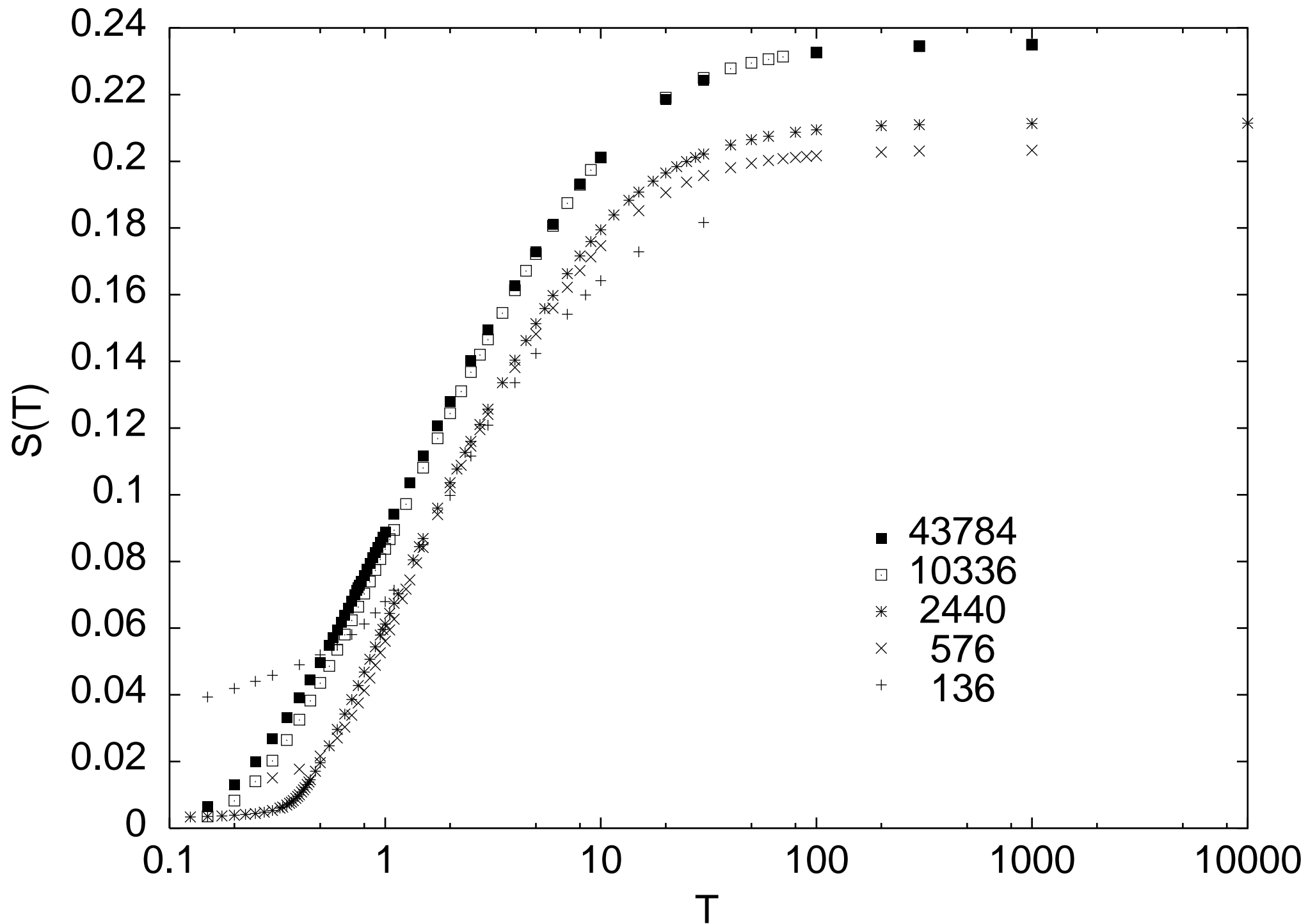
FIG. 14. Radial density function (RDF) of the rhombohedra lattice points. The peaks represent the values for the ideal tiling, the crosses denote the difference for the random tiling at $T = \infty$.

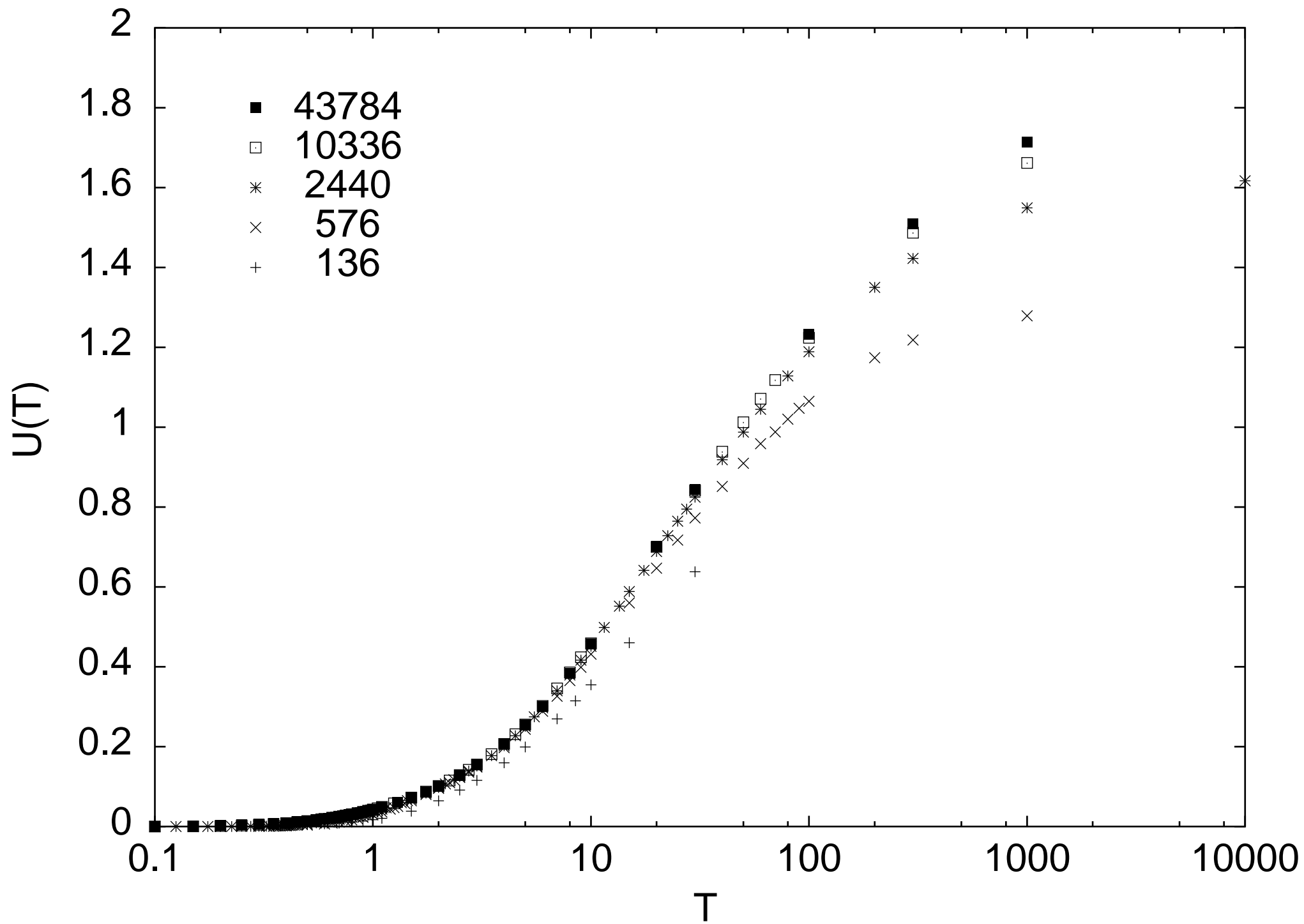


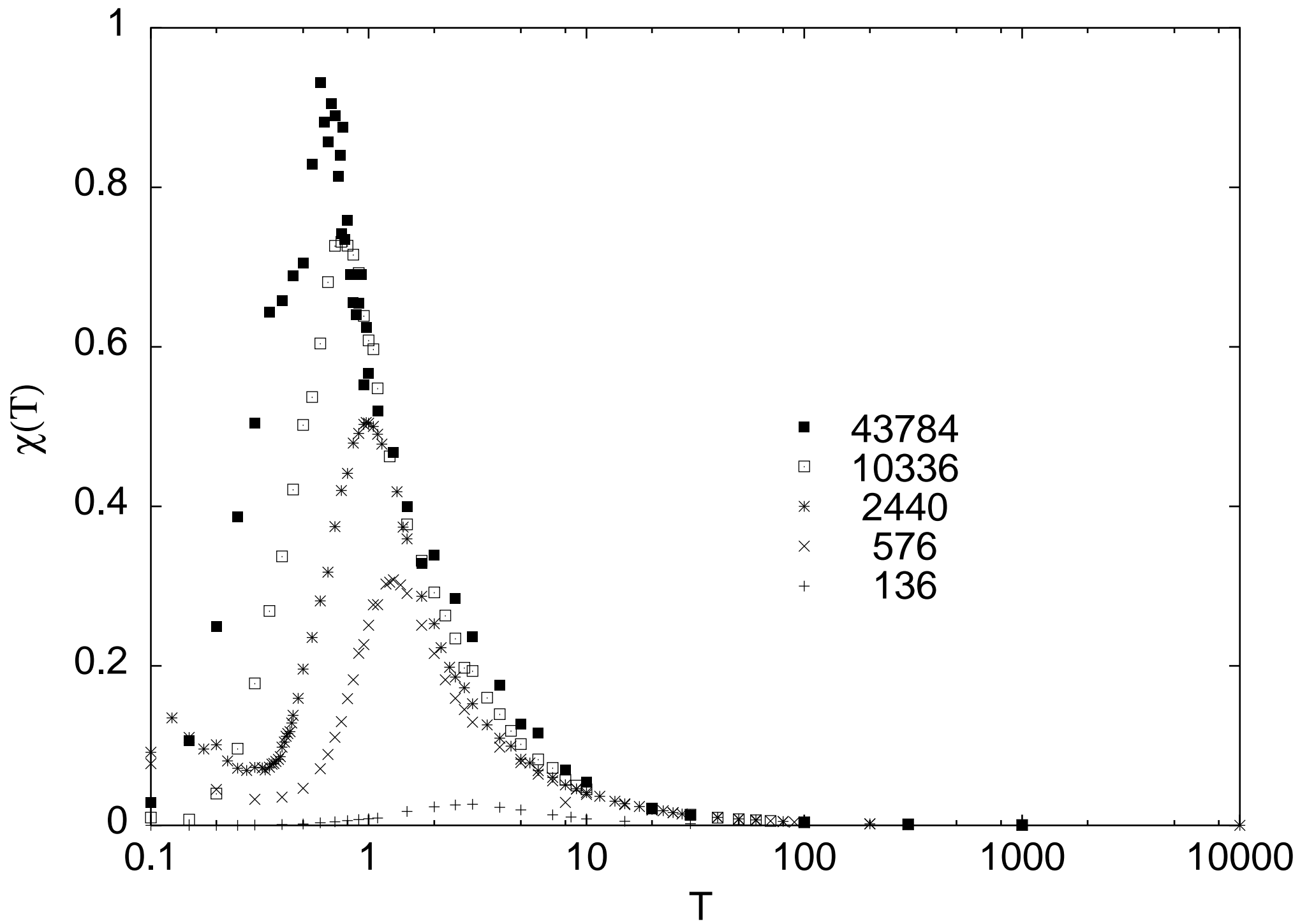


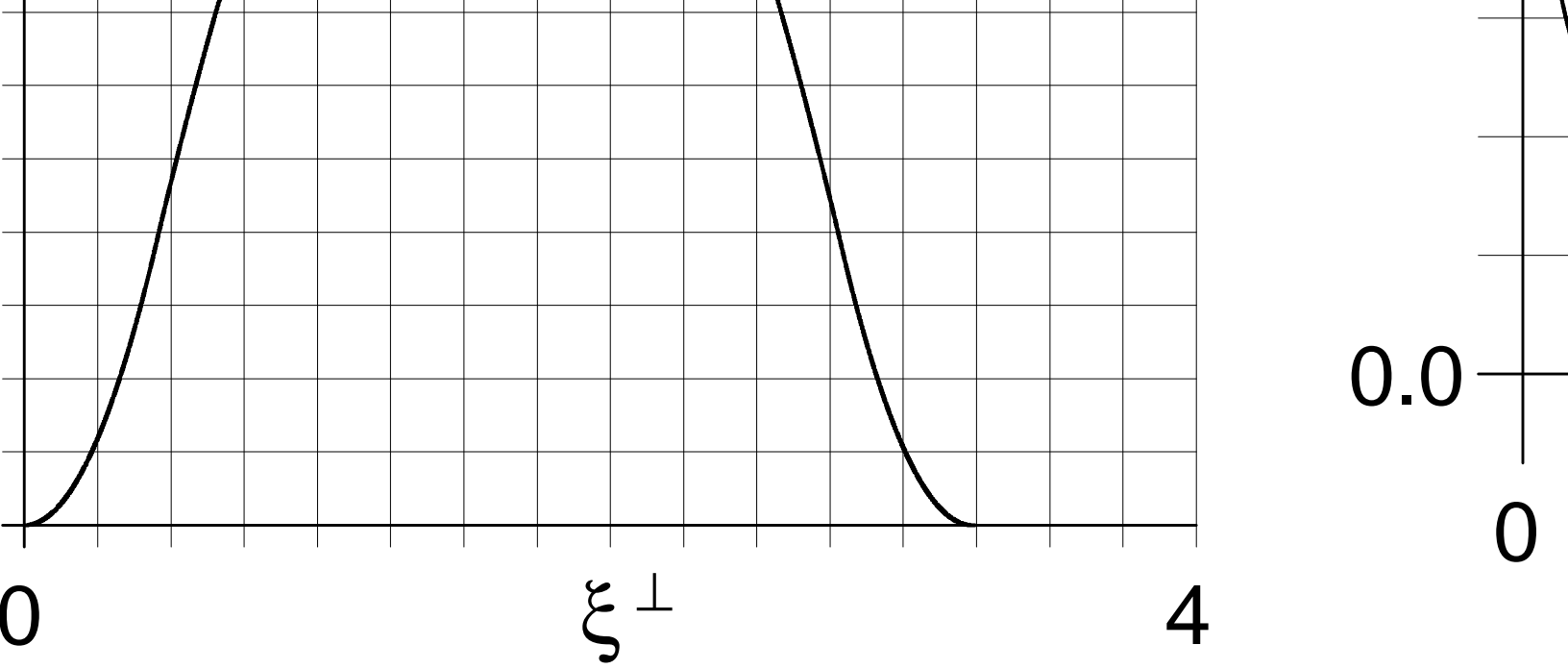












three-fold dire

